LBL-20836
Preprint c.2

# Lawrence Berkeley Laboratory

UNIVERSITY OF CALIFORNIA

RECEIVED
LAWRENCE
BERKELEY LABORATORY

## Materials & Molecular Research Division

JUN 30 1986

LIBRARY AND
DOCUMENTS SECTION

Submitted to Ultramicroscopy

ON THE INCLUSION OF UPPER LAUE LAYERS
IN COMPUTATIONAL METHODS IN HIGH RESOLUTION
TRANSMISSION ELECTRON MICROSCOPY

R. Kilaas, M.A. O'Keefe, and K.M. Krishnan

January 1986

TWO-WEEK LOAN COPY
This is a Library Circulating Copy
which may be borrowed for two weeks

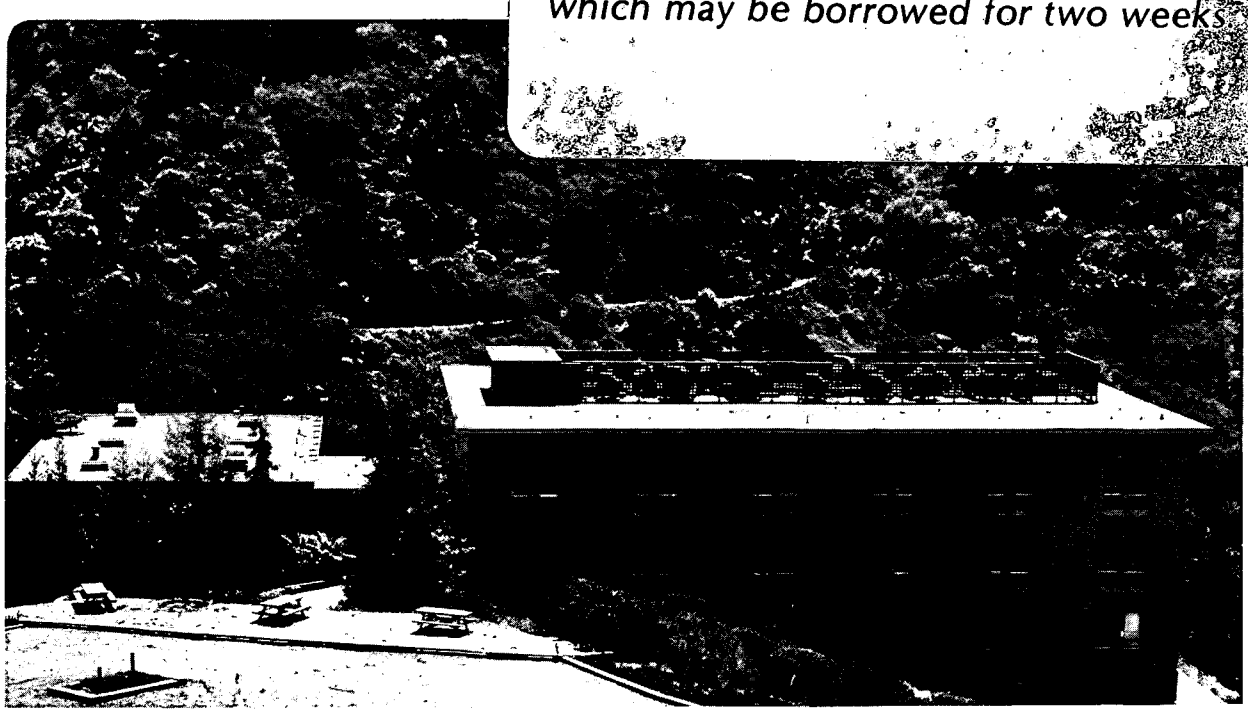

LBL-20836 c.2

Prepared for the U.S. Department of Energy under Contract DE-AC03-76SF00098

## DISCLAIMER

This document was prepared as an account of work sponsored by the United States Government. While this document is believed to contain correct information, neither the United States Government nor any agency thereof, nor the Regents of the University of California, nor any of their employees, makes any warranty, express or implied, or assumes any legal responsibility for the accuracy, completeness, or usefulness of any information, apparatus, product, or process disclosed, or represents that its use would not infringe privately owned rights. Reference herein to any specific commercial product, process, or service by its trade name, trademark, manufacturer, or otherwise, does not necessarily constitute or imply its endorsement, recommendation, or favoring by the United States Government or any agency thereof, or the Regents of the University of California. The views and opinions of authors expressed herein do not necessarily state or reflect those of the United States Government or any agency thereof or the Regents of the University of California.

LBL-20836

# ON THE INCLUSION OF UPPER LAUE LAYERS IN COMPUTATIONAL METHODS IN HIGH RESOLUTION TRANSMISSION ELECTRON MICROSCOPY

*Roar Kilaas, Michael A. O'Keefe*
*and Kannan M. Krishnan*

National Center for Electron Microscopy
Lawrence Berkeley Laboratory
University of California
Berkeley, California 94720

Submitted to

*Ultramicroscopy*

January 1986

# On the Inclusion of Upper Laue Layers in Computational Methods In High Resolution Transmission Electron Microscopy

**Abstract**

Three different methods for computing scattering amplitudes in High Resolution Transmission Electron Microscopy (HRTEM) have been investigated as to their ability to include upper Laue layer (ULL) interaction. The conventional first order multislice method using fast Fourier transform (FFT) and the second order multislice method (SOM method) are shown to yield calculated intensities of first order Laue reflections with the use of slice thicknesses smaller than the crystal periodicity along the incident electron beam direction. It is argued that the calculated intensities of ULL reflections approach the correct values in the limiting case of vanishing slice thickness and electron wavelength. The third method, the improved phasegrating method (IPG) does also in principle include ULL effects, but is severely limited as to choice of slice thickness and sampling interval.

A practical way to use slice thicknesses less than the crystal periodicity along the incident beam direction is shown for both the conventional FFT method and the second order multislice method and tested on a spinel structure. It is also shown that the IPG method does not easily allow for a slice thickness different from the crystal periodicity in the beam direction.

## 1. Introduction

Because of the small curvature of the Ewald sphere most electrons scatter into directions given by the reciprocal lattice points lying in the zero order Laue zone (ZOLZ) (Fig. 1). Diffraction into upper Laue layers is a small effect, but is easily observed in Convergent Beam Electron Diffraction (CBED). The ULL reflections do not contribute directly to the image in HRTEM since the effective aperture, whether a real objective aperture or a virtual aperture defined by an envelope function [1], exclude the contribution to the image from the ULL beams. In most cases, however, because of dynamical scattering the ULL reflections will modify the intensity of the zero order Laue reflections and consequently affect the image. Where such ULL interactions are no longer negligible they must be included in the computation of electron micrographs to give more accurate results.

For practical reasons most image simulations in HRTEM employ a method based on multislicing. In this computation the specimen is considered to be sectioned into slices perpendicular to the electron beam and the electron wave function is calculated at every slice in a recursive way starting from the known electron distribution at the beginning of the first slice. Again for practical reasons, the crystal periodicity parallel to the electron beam is invariably chosen as the slice thickness provided it does not violate the criteria of validity for these multislice methods, [2],[3].

Various methods to include the effect of the ULL have been suggested. These are:

1. The use of slices smaller than the crystal periodicity parallel to the direction of the incoming electron beam [2],[4].

2. Second order multislice, using potential eccentricity within the slice [5].

3. Improved phasegrating method [6].

So far the degree of success of these methods in including ULL interactions have not been shown. It is generally believed that as the variation of the crystal potential along the incident electron beam direction is taken into account, the ULL reflections are automatically included. The degree to which this is correct is the topic of this paper.

The 200 reflections in the stoichiometric spinel, $MgAl_2O_4$ [001], described by the space group Fd3m ($O_h^7$) [7] are kinematically forbidden. However Steeds has shown that they appear in experimental convergent beam electron diffraction patterns [8] and accredits [9] their presence to scattering from the first order Laue zone (FOLZ). This being the case, the ability to account for their presence would serve as a test for the inclusion of ULL effects in present multislice calculations.

Additionally, with the use of small slice thicknesses it is of utmost importance that one correctly takes into account the potential for each slice in each of the three multislice calculations. Different authors approach this problem in different ways, not all equivalent and unfortunately not all correct, and this paper will address this question.

## 2. Theory

The three multislice formulations that will be discussed are all approximations to the solution of the modified Schrodinger equation below [5]

$$\frac{\partial \phi}{\partial z} = i\sigma V\phi + \frac{i\lambda}{4\pi} \nabla_\perp^2 \phi \tag{2.1}$$

where

$$\sigma = \frac{2\pi m e \lambda}{h^2} \tag{2.2}$$

and

$$\nabla_{\perp}^2 = \frac{\partial^2}{\partial x^2} + \frac{\partial^2}{\partial y^2} \tag{2.3}$$

V is the crystal potential in volts.

## 2.1 Conventional Multislice with Small Slice Thicknesses

The conventional multislice formulation involves a recursive application of the following equation:

$$\phi(x,y,z_m + \Delta z) = P(x,y,\Delta z) * [Q(x,y,z_m,\Delta z) \cdot \phi(x,y,z_m)] \tag{2.1.1}$$

where P(x,y,z) is the free space propagator, and Q(x,y,z,Δz) is called the phasegrating. The expressions for P and Q are:

$$Q(x,y,z_m,\Delta z) = \exp\left\{ i\sigma \int_{z_m}^{z_m+\Delta z} V(x,y,z)dz \right\} \tag{2.1.2}$$

$$P(x,y,\Delta z) = -\frac{i}{\lambda \Delta z} \exp\left\{ \frac{i\pi}{\lambda \Delta z} (x^2 + y^2) \right\} \tag{2.1.3}$$

All information about the scattering potential is contained in Q and only reflections allowed by the Fourier transform of Q are possible. Similarly all the information about the curvature of the Ewald sphere is contained in the propagator the function of which is to keep track of the excitation errors of each reflection (in the zero order Laue zone), see Appendix A.

If the crystal periodicity (c) parallel to the electron beam is used as a slice thickness i.e. Δz = c, then only reciprocal lattice points in the ZOLZ together with the

corresponding structure factors determine the allowed reflections, as shown below.

It is customary to define a "projected" potential as follows :

$$V_b(x,y,z_m,\Delta z) \equiv \frac{1}{\Delta z}\int_{z_m}^{z_m+\Delta z} V(x,y,z)dz \tag{2.1.4}$$

$$= \frac{1}{\Delta z}\int_{z_m}^{z_m+\Delta z} \sum_{h,k,\ell} V(h,k,\ell)e^{2\pi i(\frac{hx}{a}+\frac{ky}{b}\frac{+\ell z}{c})}dz$$

where V has been expressed as a Fourier series. The $V(h,k,\ell)$'s are calculated by performing a sum over all atoms within the unit cell

$$V(h,k,\ell) = \frac{h^2}{2\pi meV_c}\sum_i \mathscr{F}_i(h,k,\ell)e^{-2\pi i(\frac{hx_i}{a}+\frac{ky_i}{b}+\frac{\ell z_i}{c})}dz \tag{2.1.5}$$

where $(x_i,y_i,z_i)$ is the position of atom no. i with an electron scattering factor $\mathscr{F}_i$. $V_c$ is the volume of the unit cell. Performing the integral gives ,as also pointed out by Self et al. [10] :

$$V_p(x,y,z_m,\Delta z) = \frac{1}{\Delta z}\sum_{h,k,\ell} V(h,k,\ell)e^{2\pi i(\frac{hx}{a}+\frac{ky}{b})}\frac{\sin\pi\ell\Delta z/c}{\pi\ell/c}e^{2\pi i\ell z_{mo}/c} \tag{2.1.6}$$

where $z_{mo} \equiv z + \Delta z/2$

Setting $\Delta z = c/n$ gives the following expression for the projected potential

$$V_p(z_m,\Delta z=c/n) = \sum_{h,k,\ell} V(h,k,\ell)e^{2\pi i(\frac{hx}{a}+\frac{ky}{b})}\frac{\sin\pi\ell/n}{\pi\ell/n}e^{2\pi i\ell z_{mo}/c} \tag{2.1.8}$$

In the case where the crystal periodicity is used as the slice thickness, $\Delta z = c$ and $n = 1$. In this case (2.1.8) reduces to

$$V_p(z_m,\Delta z=c) = \sum_{h,k} V(h,k,o)e^{2\pi i(\frac{hx}{a}+\frac{ky}{b})} \tag{2.1.9}$$

This expression shows that for $n = 1$, only the components of the potential with a reciprocal vector lying in the ZOLZ contribute to the scattering. Thus no ULL effects

can enter in the calculation. If, however n is not 1, the expression for the projected potential is a sum over all reciprocal vectors with a weighting factor proportional to the Fourier coefficient of the crystal potential [10] [11]. In principle this should allow for dynamical scattering between all (hk$\ell$) reflections and thus automatically account for ULL effects. Whether this is accurate or not will be addressed later in section 5.

Previously the projected potential has been calculated in several ways:

i) Calculate the projected potential for a slice of thickness c. If a slice thickness of c/n is to be used, then simply divide the previously calculated potential by n and use this as the projected potential for each slice.

ii) Divide the unit cell into n volume elements which may include atom sectioning. The projected potential for each slice is calculated from the projection of the atoms contained within the slice according to (2.1.5). The sum is carried out over the atoms contained within the slice.

iii) Calculate a three dimensional crystal potential by summing over V(hk$\ell$) and using a three-dimensional. Fourier transform to find V(x,y,z). With modern computers the integral over V from z to z + $\Delta$z can easily be performed.

The first approach is obviously incorrect. The second method would be correct if it were not for the fact that the crystal potential is periodic in c and not in c/n. The third method is correct, but is impractical in cases where large unit cells are considered because of the huge amount of computer memory ($128^3$ = 8Mbytes) that is needed to store a three dimensional potential.

A practical method to calculate the projected potential for each slice is based on (2.1.6) and thus doesn't require additional memory. Starting from (2.1.6) one

calculates the projected potential by first summing over $\ell$. One can write

$$V_p(x,y,z_m,n) = \sum_{h,k} V'_{z_m,n}(h,k) e^{2\pi i(\frac{hx}{a}+\frac{ky}{b})} \tag{2.1.10}$$

where

$$V'_{z_m,n}(h,k) \equiv \sum_{\ell} V(h,k,\ell) \frac{\sin \pi\ell/n}{\pi\ell/n} e^{2\pi i \ell z_{mo}/c} \tag{2.1.11}$$

This amounts to modifying all V(h,k,0) by adding in a contribution from the ULL, as shown in Fig. 1. Thus reflections that were forbidden by V(h,k,0) may now be allowed by V′(h,k,0). The intensity of forbidden reflections will be zero for thicknesses corresponding to a multiple of unit cell distances c, only if there is a complete cancellation from the contents of the unit cell.

This yields an effective algorithm for dividing the specimen up into slices smaller than c. First, the coefficients $V(h,k,\ell)$ should be formed by summing over all atoms within a bona fide unit cell with a periodicity c along the incident beam direction. Secondly, if there are n "sub-slices", it is necessary to calculate n separate phasegratings or projected potentials according to (2.1.8), where for a given n, only $Z_{mo}$ will change from sub-slice to sub-slice. The most efficient way to generate the n phasegratings depends on available computer memory.

## 2.2 Second Order Multislice

This method goes one step further and aspires to include ULL effects within the slice. Developed by Van Dyck [5] it introduces the concept of potential eccentricity within each slice. The equivalent to (2.1.1) is the recursive operation:

$$\phi(x,y,z_m+\Delta z) = e^{\frac{1}{2}i\sigma\Delta z(1+\delta)V_p} e^{\frac{i\lambda\Delta z}{4\pi}\nabla_\perp^2} e^{\frac{1}{2}i\sigma\Delta z(1-\delta)V_p} \phi(x,y,z_m) \tag{2.2.1}$$

where the potential eccentricity $\delta$ is given as

$$\delta = \delta_m(x,y) \equiv \frac{\overline{z}_m(x,y) - \Delta z/2}{\Delta z/2} \tag{2.2.2}$$

The average quantity z is defined as

$$\overline{z}_m(x,y) \equiv \int_{z_m}^{z_m+\Delta z} (z - z_m)\, V(x,y,z)dz \tag{2.2.3}$$

In an evaluation of the real space method, Kilaas & Gronsky [3], used the above recursive operation to calculate both projected potentials and potential eccentricities from the three-dimensional crystal potential. However, the expressions $1/2(1+\delta)V_p$ and $1/2(1-\delta)V_p$ can be calculated in a way similar to the procedure described in 2.1 for calculating the projected potential as shown below:

It is useful to first calculate the quantity

$$\begin{aligned}
\frac{1}{\Delta z} V_p \overline{z}_m &\equiv \frac{1}{\Delta z^2} \int_{z_m}^{z_m+\Delta z} (z - z_m)\, V(x,y,z)dz \\
&= \frac{1}{\Delta z^2} \int_{z_m}^{z_m+\Delta z} \sum_{h,k,\ell} (z - z_m)\, V(h,k,\ell) e^{2\pi i(\frac{hx}{a} + \frac{ky}{b} + \frac{\ell z}{c})} dz \qquad (2.2.4) \\
&= \frac{1}{\Delta z^2} \sum_{h,k} e^{2\pi i(\frac{hx}{a} + \frac{ky}{b})} \sum_{\ell} V(h,k,\ell) \frac{e^{2\pi i \ell z_{mo}/c}}{2\pi i \ell/c} \left( \Delta z\, e^{\pi i \ell \Delta z/c} - \frac{\sin \pi \ell \Delta z/c}{\pi \ell/c} \right)
\end{aligned}$$

Setting $\Delta z = c/n$ gives

$$\begin{aligned}
\frac{V_p \overline{z}_m}{\Delta z} &= \sum_{h,k} e^{2\pi i(\frac{hx}{a} + \frac{ky}{b})} \sum_{\ell} V(h,k,\ell) \frac{n}{2\pi i \ell} e^{2\pi i \ell z_{mo}/c} \left( e^{\pi i \ell z_{mo}/c} - \frac{\sin \pi \ell/n}{\pi \ell/n} \right) \qquad (2.2.5) \\
&\equiv \sum_{h,k} V_{\overline{z}}(h,k) e^{2\pi i(\frac{hx}{a} + \frac{ky}{b})}
\end{aligned}$$

One can now write:

$$\tfrac{1}{2}(1+\delta)V_p = \frac{\overline{z}V_p}{\Delta z} = \sum_{h,k} V_{\overline{z}}(h,k)e^{2\pi i(\frac{hx}{a}+\frac{ky}{b})} \tag{2.2.6}$$

$$\tfrac{1}{2}(1-\delta)V_p = V_p - \frac{\overline{z}V_p}{\Delta z} = \sum_{h,k} [V'(h,k) - V_{\overline{z}}(h,k)]\, e^{2\pi i(\frac{hx}{a}+\frac{ky}{b})} \tag{2.2.7}$$

## 2.3 Improved Phasegrating Method

This method, again suggested by Van Dyck [6], is based upon a modulated phasegrating. The effect of the potential is considered larger than the effect of the propagator which is treated as a perturbation. In this case the wavefunction is written

$$\phi(x,y,z) = \exp\left\{ i\sigma\int_o^z V(x,y,z')dz' \right\} \theta(x,y,z) \tag{2.3.1}$$

Substituting the above expression into the equation for $\phi$ (2.1) gives

$$\theta(x,y,z) = \theta(x,y,o) + \frac{i\lambda}{4\pi}\int_o^z dz' \Big\{ \nabla_\perp^2\theta(z') + i\sigma\Delta z[\nabla_\perp^2 V_p(z')]\theta(z') \tag{2.3.2}$$

$$+ 2i\sigma\Delta z\nabla_\perp V_p(z')\cdot\nabla_\perp\theta(z') + (i\sigma\Delta z)^2\,\theta(z')[\nabla_\perp V_p(z')]^2 \Big\}$$

which yields a first order perturbation result for theta

$$\theta(z) \approx \theta(o) + \frac{i\lambda\Delta z}{4\pi}\Bigg\{ \nabla_\perp^2\theta(o) + i\sigma\Delta z\theta(o)\int_o^z dz' \tag{2.3.3}$$

$$[\frac{1}{\Delta z}\nabla_\perp^2 V_p + i\sigma\Delta z\frac{1}{\Delta z}(\nabla_\perp V_p)^2] + 2i\sigma\Delta z\nabla_\perp\theta(o)\cdot\int_o^z dz'\,\frac{1}{\Delta z}\nabla_\perp V_p \Bigg\}$$

A practical application of (2.3.3) can be formulated as follows: One considers a multislice approach where the specimen is divided into N slices perpendicular to the incident electron beam. The wavefunction after the first slice of thickness $\Delta z$ is writ-

ten

$$\phi(x,y,\Delta z) = \exp\{i\sigma\Delta z V_p(\Delta z)\}\theta(\Delta z) \tag{2.3.4}$$

For N slices of thickness $\Delta z$ (2.3.4) becomes

$$\phi(x,y,N\Delta z) = \exp\left\{ i\sigma \int_0^{N\Delta z} V(x,y,z') \right\}\theta(N\Delta z) \tag{2.3.5}$$

where $\theta$ $(N\Delta z)$ is a recursive application of (2.3.3).

The major problem in using (2.3.3) comes from solving for the integrals over $V_p(z)$. However, proceeding as before, one gets

$$\frac{1}{\Delta z}\int_{z_m}^{z_m+\Delta z} \nabla_\perp^2 V_p dz' = -(2\pi)^2 \sum_{h,k} e^{2\pi i(\frac{hx}{a}+\frac{ky}{b})}\left(\frac{h^2}{a^2}+\frac{k^2}{b^2}\right) \tag{2.3.6}$$

$$\times \sum_{\ell} V(h,k,\ell)\frac{n}{2\pi i\ell}\left(e^{2\pi i\ell z_{mo}/c}\frac{\sin \pi\ell/n}{\pi\ell/n} - 1\right)$$

$$\frac{1}{\Delta z}\int_{z_m}^{z_m+\Delta z} \frac{\partial V_p}{\partial x} dz' = 2\pi i \sum_{h,k} e^{2\pi i(\frac{hx}{a}+\frac{ky}{b})}\left(\frac{h}{a}\right)\sum_{\ell} V(h,k,\ell)\frac{n}{2\pi i\ell}\left(e^{2\pi i\ell z_{mo}/c}\frac{\sin \pi\ell/n}{\pi\ell/n} - 1\right) \tag{2.3.7}$$

$$\frac{1}{\Delta z}\int_{z_m}^{z_m+\Delta z} \frac{\partial V_p}{\partial y} dz' = 2\pi i \sum_{h,k} e^{2\pi i(\frac{hx}{a}+\frac{ky}{b})}\left(\frac{k}{b}\right)\sum_{\ell} V(h,k,\ell)\frac{n}{2\pi i\ell}\left(e^{2\pi i\ell z_{mo}/c}\frac{\sin \pi\ell/n}{\pi\ell/n} - 1\right) \tag{2.3.8}$$

The expression for $\int_{z_m}^{z_m+\Delta z} [(\frac{\partial V_p}{\partial x})^2 + (\frac{\partial V_p}{\partial y})^2]dz$ is given as

$$\frac{1}{\Delta z}\int_{z_m}^{z_m+\Delta z} [(\frac{\partial V_p}{\partial x})^2 + (\frac{\partial V_p}{\partial y})^2]\, dz' =$$

$$- (2\pi)^2 \sum_{\substack{h,k \\ h',k'}} \left(\frac{hh'}{a^2} + \frac{kk'}{b^2}\right) e^{2\pi i\left(\frac{h+h'}{a}x + \frac{k+k'}{b}y\right)}$$

$$\times \sum_{\ell\ell'} V(h,k,\ell)V(h',k',\ell') \frac{n}{2\pi i\ell} \frac{n}{2\pi i\ell'} \left[ e^{2\pi i(\ell+\ell')Z_{mo}/c} \frac{\sin\pi(\ell+\ell')/n}{\pi(\ell+\ell')/n} \right.$$

$$\left. - e^{2\pi i\ell Z_{mo}/c} \frac{\sin\pi\ell/n}{\pi\ell/n} - e^{2\pi i\ell' Z_{mo}/c} \frac{\sin \pi\ell'/n}{\pi\ell'/n} + 1 \right] \tag{2.3.9}$$

Equation 2.3.9 is complicated by the crossterms contained within the [ ]. In the limiting case $\Delta z/c$ goes to zero (2.3.9) simplifies to

$$\frac{1}{\Delta z} \int_{z_m}^{z_m+\Delta z} \left[\left(\frac{\partial V_p}{\partial x}\right)^2 + \left(\frac{\partial V_p}{\partial y}\right)^2\right] dz' = - \frac{(2\pi)^2}{3} \left[ \left( \sum_{h,k} \frac{h}{a} V(h,k,0) e^{2\pi i\left(\frac{hx}{a} + \frac{ky}{b}\right)} \right)^2 \right.$$

$$\left. + \left( \sum_{h,k} \frac{k}{b} V(h,k,0) e^{2\pi i\left(\frac{hx}{a} + \frac{ky}{b}\right)} \right) \right] \tag{2.3.10}$$

The other simplifying case is $\Delta z = c$. In this case one obtains as follows

$$\frac{1}{c} \int_{z_m}^{z_m+c} \nabla_\perp^2 V_p dz' = - (2\pi)^2 \sum_{h,k} e^{2\pi i\left(\frac{hx}{a} + \frac{ky}{b}\right)} \left(\frac{h^2}{a^2} + \frac{k^2}{b^2}\right) \tag{2.3.11}$$

$$\times \left[ \left(\tfrac{1}{2} + \frac{z_m}{c}\right) V(h,k,0) - \sum_{\ell \neq 0} V(h,k,\ell) \frac{n}{2\pi i\ell} \right]$$

$$\frac{1}{c} \int_{z_m}^{z_m+c} \frac{\partial V_p}{\partial x} dz' = 2\pi i \sum_{h,k} e^{2\pi i\left(\frac{hx}{a} + \frac{ky}{b}\right)} \left(\frac{h}{a}\right) \left[ \left(\tfrac{1}{2} + \frac{z_m}{c}\right) V(h,k,0) - \sum_{\ell \neq 0} V(h,k,\ell) \frac{n}{2\pi i\ell} \right] \tag{2.3.12}$$

$$\frac{1}{c} \int_{z_m}^{z_m+c} \frac{\partial V_p}{\partial y} dz' = 2\pi i \sum_{h,k} e^{2\pi i\left(\frac{hx}{a} + \frac{ky}{b}\right)} \left(\frac{k}{b}\right) \left[ \left(\tfrac{1}{2} + \frac{z_m}{c}\right) V(h,k,0) - \sum_{\ell \neq 0} V(h,k,\ell) \frac{n}{2\pi i\ell} \right] \tag{2.3.13}$$

$$\frac{1}{c}\int_{z_m}^{z_m+c}\left(\frac{\partial V_p}{\partial x}\right)^2 dz' = \left[\tfrac{1}{3}+\frac{z_m}{c}\left(1+\frac{z_m}{c}\right)\right]\left[\sum_{h,k} 2\pi i\left(\frac{h}{a}\right)V(h,k,0)e^{2\pi i\left(\frac{hx}{a}+\frac{ky}{b}\right)}\right]^2$$

$$+\,2\left[\sum_{h,k} 2\pi i\left(\frac{h}{a}\right)V(h,k,0)e^{2\pi i\left(\frac{hx}{a}+\frac{ky}{b}\right)}\right]\left[\sum_{h,k} 2\pi i\left(\frac{h}{a}\right)e^{2\pi i\left(\frac{hx}{a}+\frac{ky}{b}\right)}\sum_{\ell\neq 0}\left(\frac{1}{2\pi i\ell}\right)^2 V(h,k,\ell)\right]$$

$$+\left(\tfrac{1}{2}+\frac{z_m}{c}\right)\left[\sum_{h,k} 2\pi i\left(\frac{h}{a}\right)V(h,k,0)e^{2\pi i\left(\frac{hx}{a}+\frac{ky}{b}\right)}\right]$$

$$\times\left[\sum_{h,k} 2\pi i\left(\frac{h}{a}\right)e^{2\pi i\left(\frac{hx}{a}+\frac{ky}{b}\right)}\sum_{\ell\neq 0}\frac{i}{2\pi\ell}V(h,k,\ell)\right] \qquad (2.3.14)$$

$$+\left[\sum_{h,k} 2\pi i\left(\frac{h}{a}\right)e^{2\pi i\left(\frac{hx}{a}+\frac{ky}{b}\right)}\sum_{\ell\neq 0}\frac{1}{2\pi i\ell}V(h,k,\ell)\right]^2$$

The expression for the integral $\int\left(\frac{\partial V_p}{\partial y}\right)^2 dz$ follows from (2.3.14).

## 3. Procedure

Computer programs to implement the various methods were written according to the theory outlined in paragraph 2. and applied to the test case of a crystal of $MgAl_2O_4$, spinel (space group Fd3m, a = b c = 8.08 Å) oriented in [001]. In the case of the improved phasegrating method only $\Delta z$ = c was considered since this was the only case that allowed the expression given by (2.3.9) to be calculated in a reasonable time. As with the conventional multislice method and the second order multislice method, slice thicknesses of 8.08 Å, 4.04 Å, 2.02 Å and 1.01 Å were used, corresponding to n = 1,2,4 and 8 respectively.

## 4. Results

The results of the computations are given in Figs. 2 through 5. Figure 2 shows amplitudes for the central beam and the reflections 110, 200, 220 and 400 for a slice thickness of 8.08 Å, 2.02 Å and 1.01 Å calculated by the conventional multislice (FFT) method, while Fig. 3 shows the corresponding results calculated by the second order multislice method. The accelerating voltage is 200 kV and all reflections out to 4.0 $Å^{-1}$ were included in the calculations. The improved phasegrating method failed to produce reasonable results for this structure in the case of $\Delta z = c$ and $g_{max} = 4.0$ $Å^{-1}$ (see Discussion).

The 110 reflection is forbidden both kinematically and dynamically by the FCC structure and has zero amplitude for any thickness when $\Delta z = c$. The 200 is forbidden by reflections within the ZOLZ, but is seen as pairs of bright lines symmetrical around the exact Bragg position and separated by a few milliradians in CBED patterns through dynamical scattering from the first order Laue zone [9]. The calculations however, are for a parallel incident beam and do not show any significant amount of scattering into the 200 reflection (compared to the 110 reflection). Within the unit cell both the amplitudes of the 110 and the 200 reflection deviate from zero, (n = 4,8) and only at thicknesses corresponding to multiples of c do they become negligibly small. The reflections are "forbidden" because scattering from one part of the unit cell interferes destructively with scattering from another part of the unit cell. Only if the cancellation is complete, which would require that the electron wavefunction for all scattering purposes remains the same throughout the cell, does the amplitude go to zero.

Figures 4 and 5 show four diffraction patterns calculated from a 300 Å thick crystal of $MgAl_2O_4$. In a) the slice thickness is c, while in b), c) and d) the slice thickness

is c/2, c/4 and c/8 respectively. The results in Fig. 4 are for the FFT method while the results in Fig. 5 are for the SOM method.

## 5. Discussion

The failure to give reasonable results by the improved phasegrating method is caused by the large slice thickness required to perform the calculation [12]. Because of the necessarily large $g_{max}$ that must be used, the computation cannot be performed within the domain of validity for this method. Kilaas [12] shows that the criteria for validity of the IPG are more severe than that of the real space method.

With the incident beam down the zone axis, both the first order FFT method and the second order multislice method fail to indicate any scattering into the 200 reflections from out of the ZOLZ. Published [001] spinel CBED patterns (e.g., [9]) show pairs of white lines in the 200 spots, with separations of about one tenth of the 000–220 distance at 100 keV. This means that crystal tilts (or incident beam misalignments) of the order of 0.7 milliradian would be sufficient to produce significant intensity in the 200 spots in diffraction calculations that include ULL interactions. Since many HREM studies are convergent incident electron beams with semiangles of up to one milliradian, such contributions to the image need to be considered in any accurate image simulation. In the case of [001] spinel, for example, the bright 200 lines could be expected to contribute pairs of 200 fringes to the image, even though the 200 reflections are forbidden, thus producing an image with a different symmetry from that expected. A systematic study of the behavior of the diffracted beams with beam tilt is under way and should apart from hopefully producing the 200 reflections at the correct tilt, make some contribution to the debate on the crystallography of spinels [13].

The circle of excited reflections showing up in Figs. 4a and 5a are not first order Laue reflections as their location in reciprocal space would indicate, but ZOLZ that are excited because the excitation error associated with these reflections become equal to 1/c corresponding to the Ewald sphere cutting through the first order Laue zone. At this point the phase in the propagator becomes $2\pi$, equivalent to an excitation error of 0. This occurs whenever $\xi(h,k,0) = 1/\Delta z$. When $\Delta z$ is reduced by setting n = 2,4,and 8 these "pseudo" ULL reflections correspond to scattering vectors larger than the maximum reciprocal vector included in the calculations and are no longer present. However a new set of reflections located on the same circle in reciprocal space now start to appear and this time they correspond to actual first order Laue reflections, (Figs. 4c,d, and 5b,c,d.) Figure 4b does not show any ULL reflections, indicating that in the case of the FFT method a slice thickness of half a unit cell is insufficient to give ULL effects in this structure. This is not true for the SOM method which show ULL reflections even for n = 2 (Fig. 5b). This can only be attributed to the use of potential eccentricity which allow for modulations within the slice. Thus even in the case of n = 4 and n = 8, where both methods show the presence of ULL reflections, it must be concluded that the SOM method is the more accurate of the two.

The degree of accuracy to which the intensities of higher order reflections have been calculated still remains to be discussed. Only as the wavelength and the slice thickness approach zero do the first order and the second order method accurately include the interactions of upper Laue layers. As pointed out in section 2 the information about the scattering potential is contained in the phasegrating while the propagator keeps track of the excitation errors. Physically, ULL scattering occurs when the Ewald sphere approaches the first order Laue layer as shown in Fig. 1, that is when the

excitation error for the corresponding reflection becomes small. From (2.1.11) and (2.2.5) it is clear that the contribution of a particular (hk$\ell$) reflection is proportional to V(hk$\ell$), the Fourier coefficient of the potential, and does not depend upon its excitation error.In the case where the Ewald sphere passes through an ULL reflection, say (1,25,1) , V(1,25,1) would be summed into V′(1,25,0) with a weighting factor which does not depend on $\xi$(1,25,1). Additionally the remaining V(1,25,$\ell$) are all summed into V′(1,25,0) regardless of their excitation error. In effect the phasegrating "sees" a flat Ewald sphere cutting through every section of the reciprocal space. When the phasegrating is convoluted with the propagator the contribution of V′(1,25,0) depends on $\xi$(1,25,0) and not on $\xi$(1,25,1). The error in the phase of the propagator for a first order Laue reflection depends on the slice thickness and the electron wavelength and is shown in Appendix A to be $2\pi\lambda^2\Delta z g_\perp^2/c$. As the wavelength and slice thickness decreases the propagator approaches its correct value and the accuracy to which the ULL are included in the FFT method and the SOM method increases.

The improved phasegrating method does not separate the effect of the potential and the Ewald sphere (through the wavelength) and should thus better allow for the inclusion of ULL interactions. However, the restriction on wavelength, slice thickness and sampling interval associated with the IPG, excludes the use of this method on the given problem. The Ewald sphere cuts through the first ULL at approx. 3.1 $Å^{-1}$ which sets a lower limit on $g_{max}$, the maximum reciprocal scattering vector that must be included in the calculations. In order to produce reasonable results, it is necessary to use a slice thickness less than 1 Å, but the complexity of the method does not readily allow for a slice thickness less than c (8.08 Å).

## 6. Conclusion

Of the three methods that are discussed in this paper, the second order multislice method is the most suited for inclusion of ULL reflections. The use of potential eccentricity permits the use of larger slice thicknesses without sacrificing the inclusion of ULL effects. The accuracy of the calculation of higher order reflections depends on both slice thickness and electron wavelength and increases as the thickness of the slice and the wavelength approach zero. This is true for both the FFT method and the SOM method. The IPG method contains 3 dimensional information even when the slice thickness equals the crystal periodicity in the electron beam direction, but the method is impractical under most conditions because of severe restrictions on sampling interval and slice thickness.

## Acknowledgement

This work is supported by the Director, Office of Energy Research, Office of Basic Energy Sciences, Materials Sciences Division of the U.S. Department of Energy under Contract No. DE-AC03-76SF00098.

## 7. References

[1] J. Frank, Optik 38 (1973) 519

[2] P. Goodman and A.F. Moodie, Acta Cryst A30 (1974) 280

[3] R. Kilaas and R. Gronsky, Ultramicroscopy 11 (1983) 289

[4] D. F. Lynch, Acta Cryst. A27 (1971) 399

[5] D. Van Dyck, J. Microscopy 119 (1980) 141

[6] D. Van Dyck, J. Microscopy 132 (1983) 31

[7] W.H. Bragg, Phil. Mag. 30 (1915) 305

[8] J.W. Steeds, Introduction to Analytical Electron Microscopy, (eds.) Hren, Goldstein, and Joy, Chapter 15, p. 387 (1979)

[9] J. W. Steeds and N. S. Evans, Proc. 38th EMSA Meeting, (1980), 188

[10] P. Self, M.A. O'Keefe, P.R. Buseck and A.E.C. Spargo, Ultramicroscopy 11(1983) 35

[11] B. F. Buxton, M.D. Shannon and J. A. Eades, Proc. 42nd EMSA Meeting (1984), 524

[12] R. Kilaas, Ultramicroscopy (submitted 1985)

[13] B.C. de Cooman and C. B. Carter, Phil. Mag. A51 (1985) 175

# FIGURE CAPTIONS

Fig. 1. Schematic drawing showing a segment of the Ewald sphere and its relation to the reciprocal lattice. The zero and the first order Laue zones are indicated in the figure. Large open circles represent reflections lying in the zero order zone, while small open circles indicate the "column" of reciprocal points whose Fourier coefficients of the potential are summed into the Fourier coefficient of the corresponding zero order reflection to give a new effective potential.

Fig. 2. Amplitude vs. thickness for the reflections 000, 110, 200, 220, and 400 for $MgAl_2O_4$ [001]. Accelerating voltage is 200 kV and the slice thickness is 8.08 Å, 2.02 Å and 1.01 Å corresponding to n = 1, 4, and 8 respectively. Calculation is by the FFT method.

Fig. 3. Same as for Fig. 2 except that the calculation is by the SOM method.

Fig. 4. Computed diffraction patterns for a 300 Å thick specimen of $MgAl_2O_4$. The calculation is by the FFT method and the slice thickness is indicated by the value of n ($\Delta z$ = 8.08 Å/n).

Fig. 5. The same as for Fig. 4 except that the calculation is by the SOM method.

Fig. 6. Schematic drawing illustrating the central beam ($\mathbf{k}_0$) and a scattered beam ($\mathbf{k}_1$) traversing a slice of thickness $\Delta z$.

Fig. 7. Schematic drawing showing two scattered beams; one corresponding to scattering in the zero order zone and one corresponding to scattering into the first order zone.

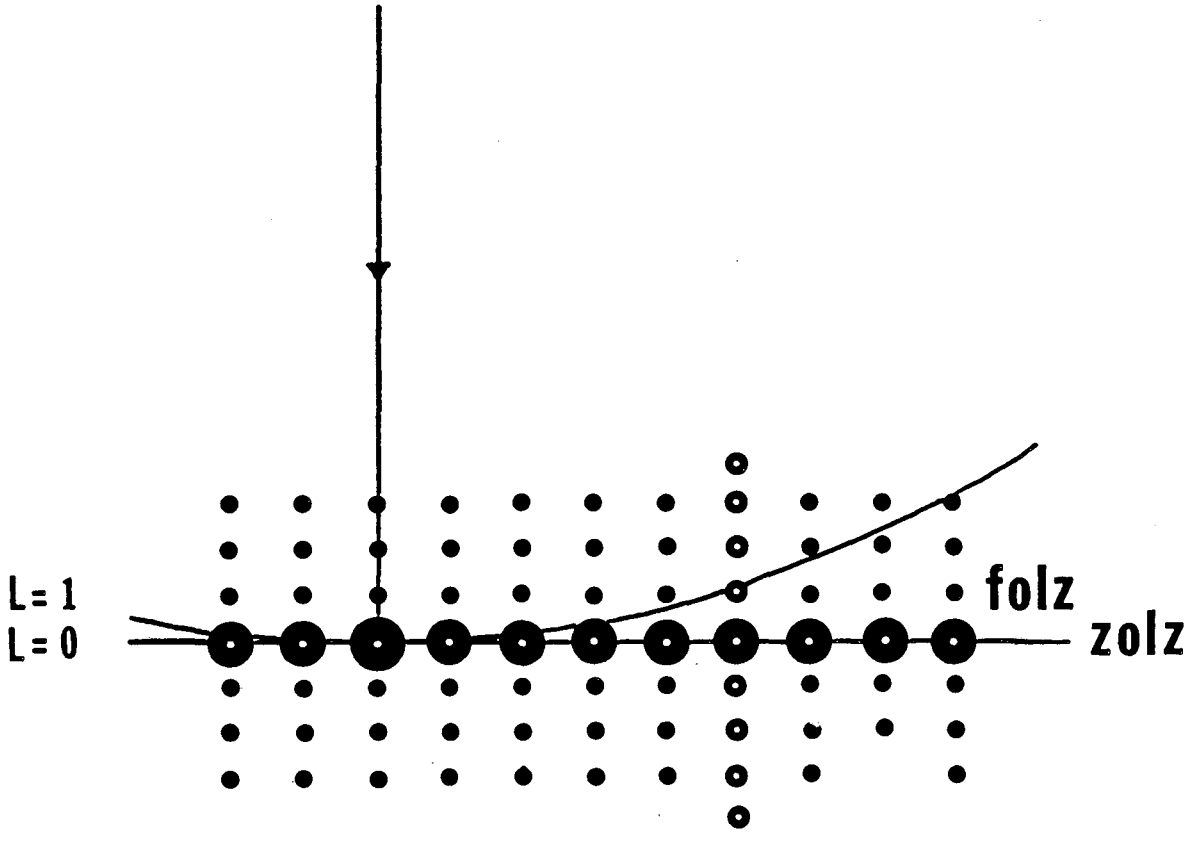


XBL 851-980

Figure 1

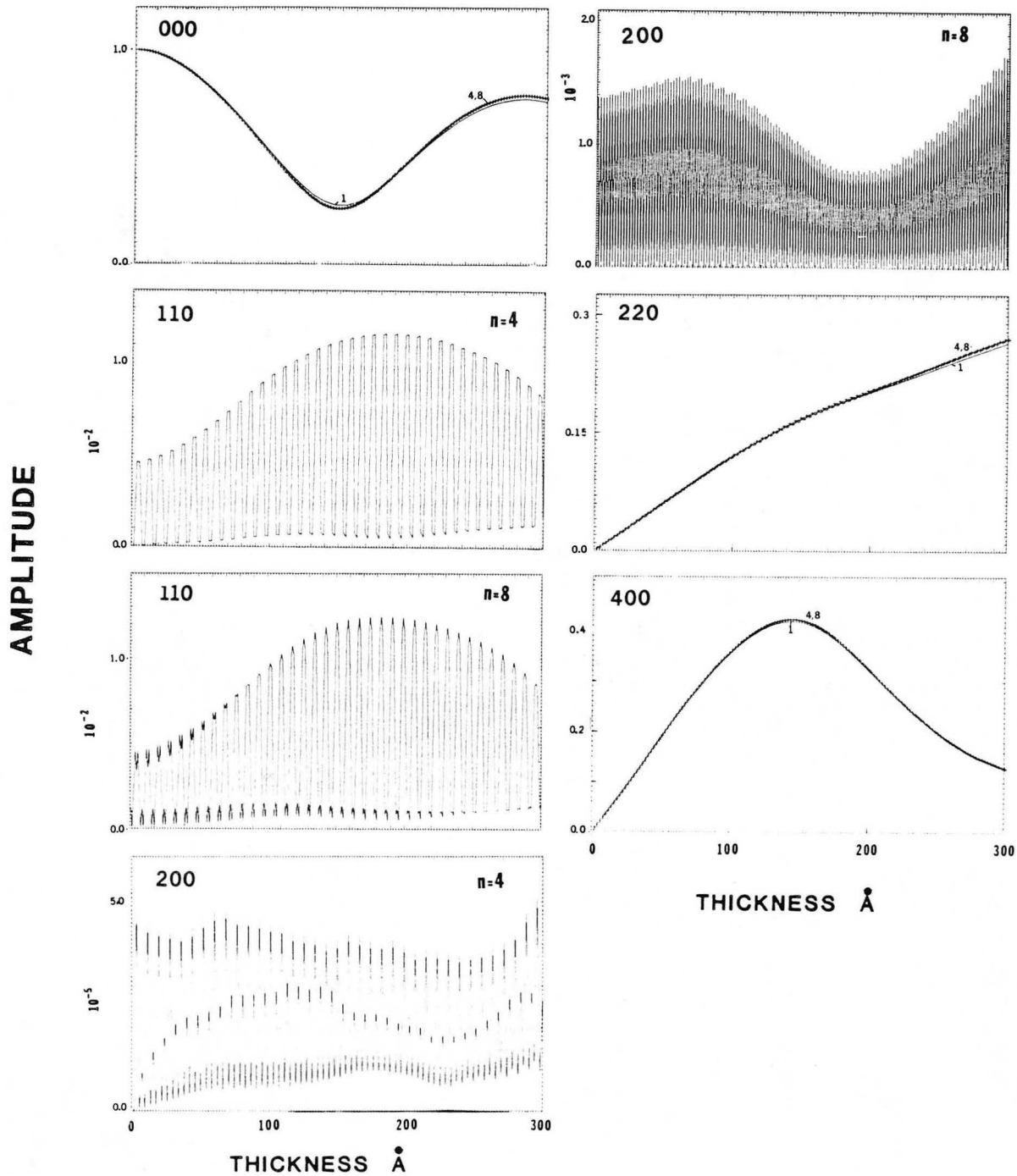


XBL 851-982

Figure 2

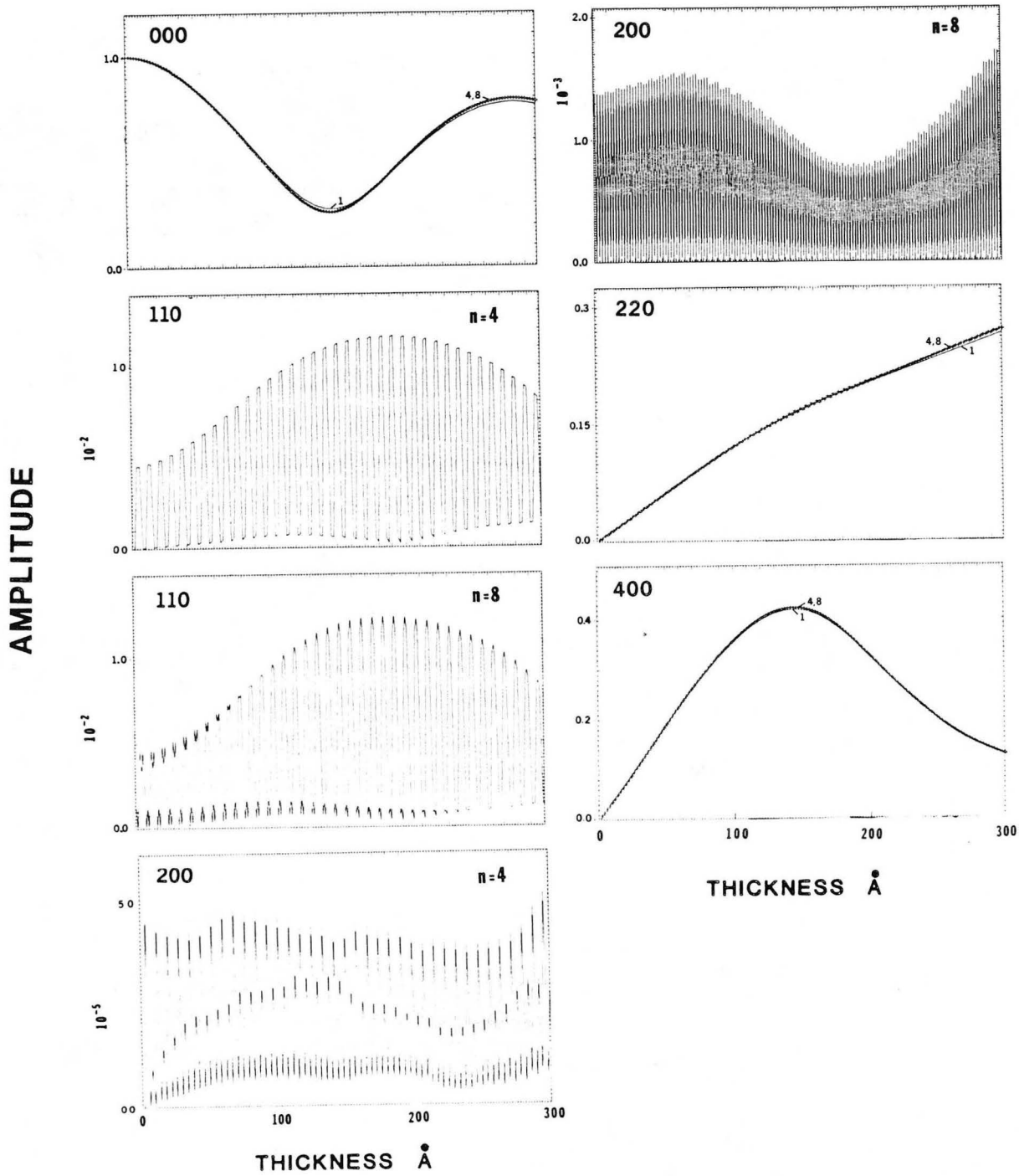


XBL 851-983

Figure 3

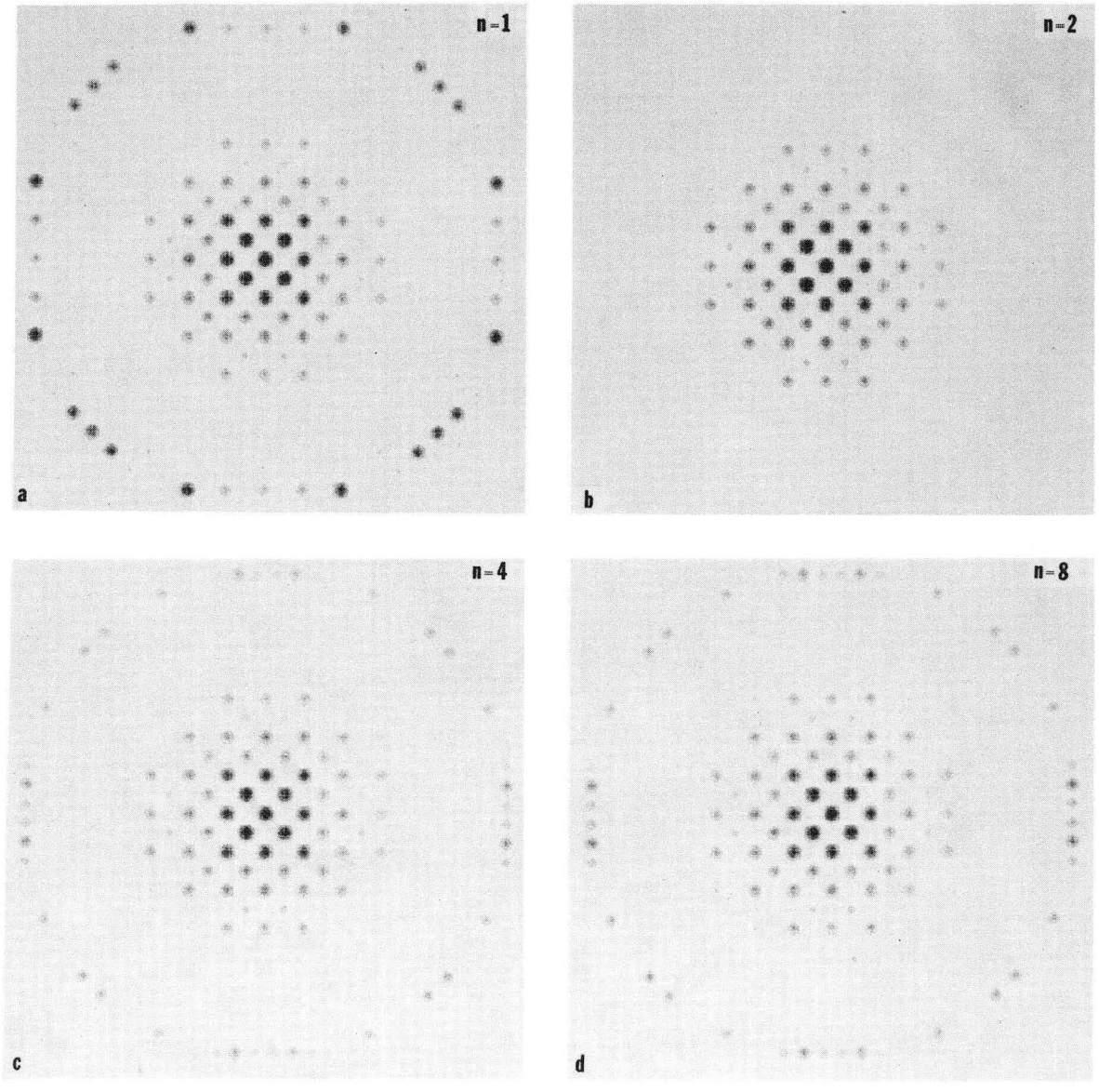


XBB 851-793

Figure 4

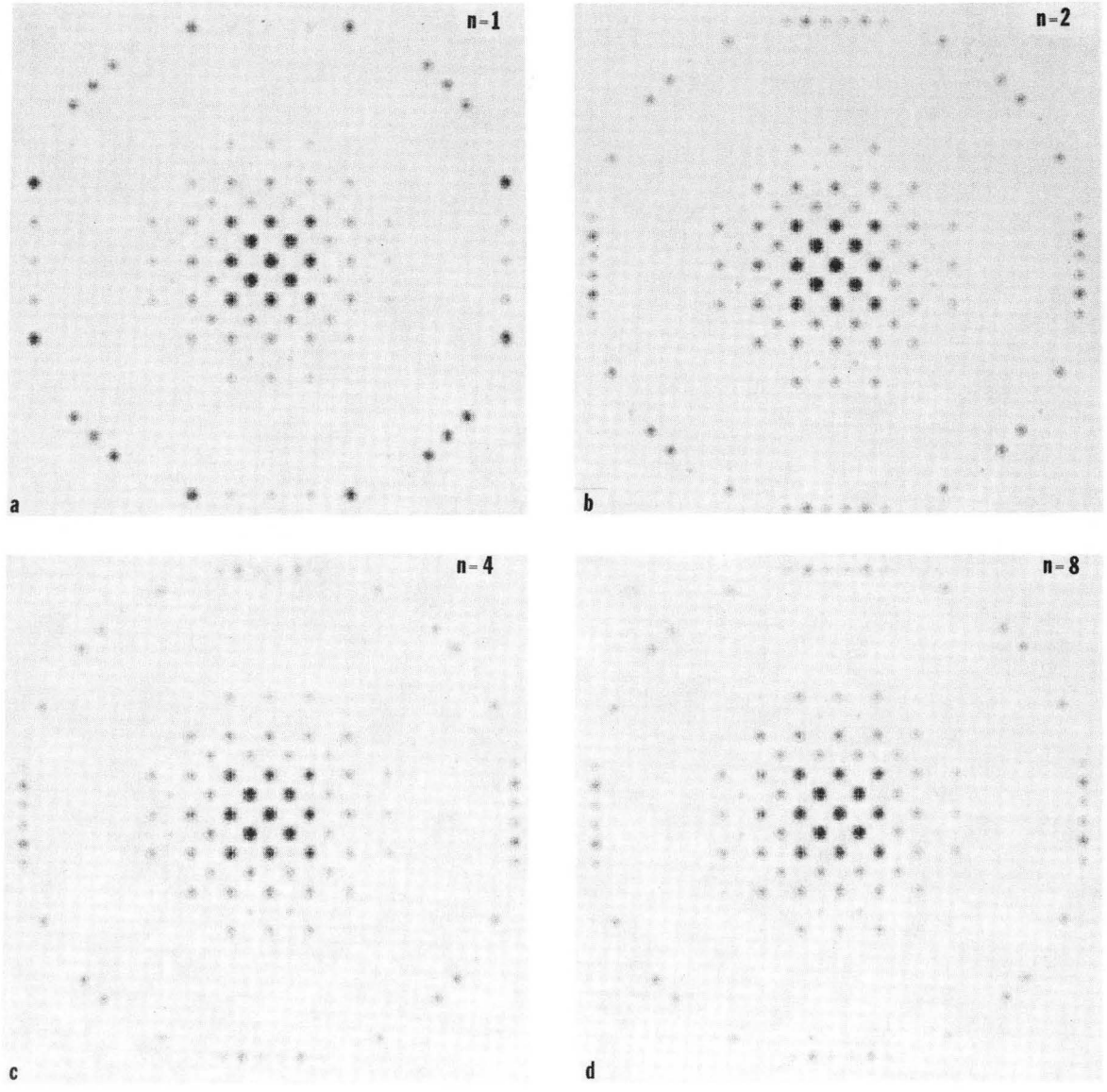


XBB 851-792

Figure 5

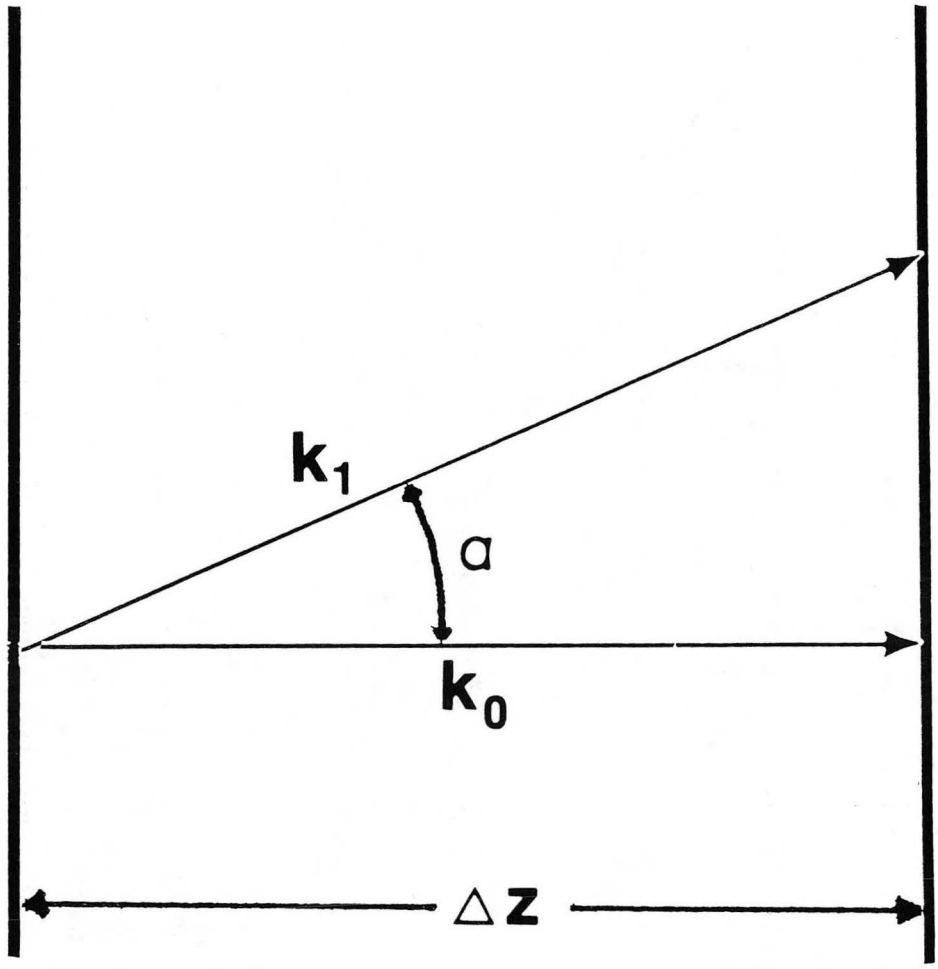


XBL 851-979

Figure 6

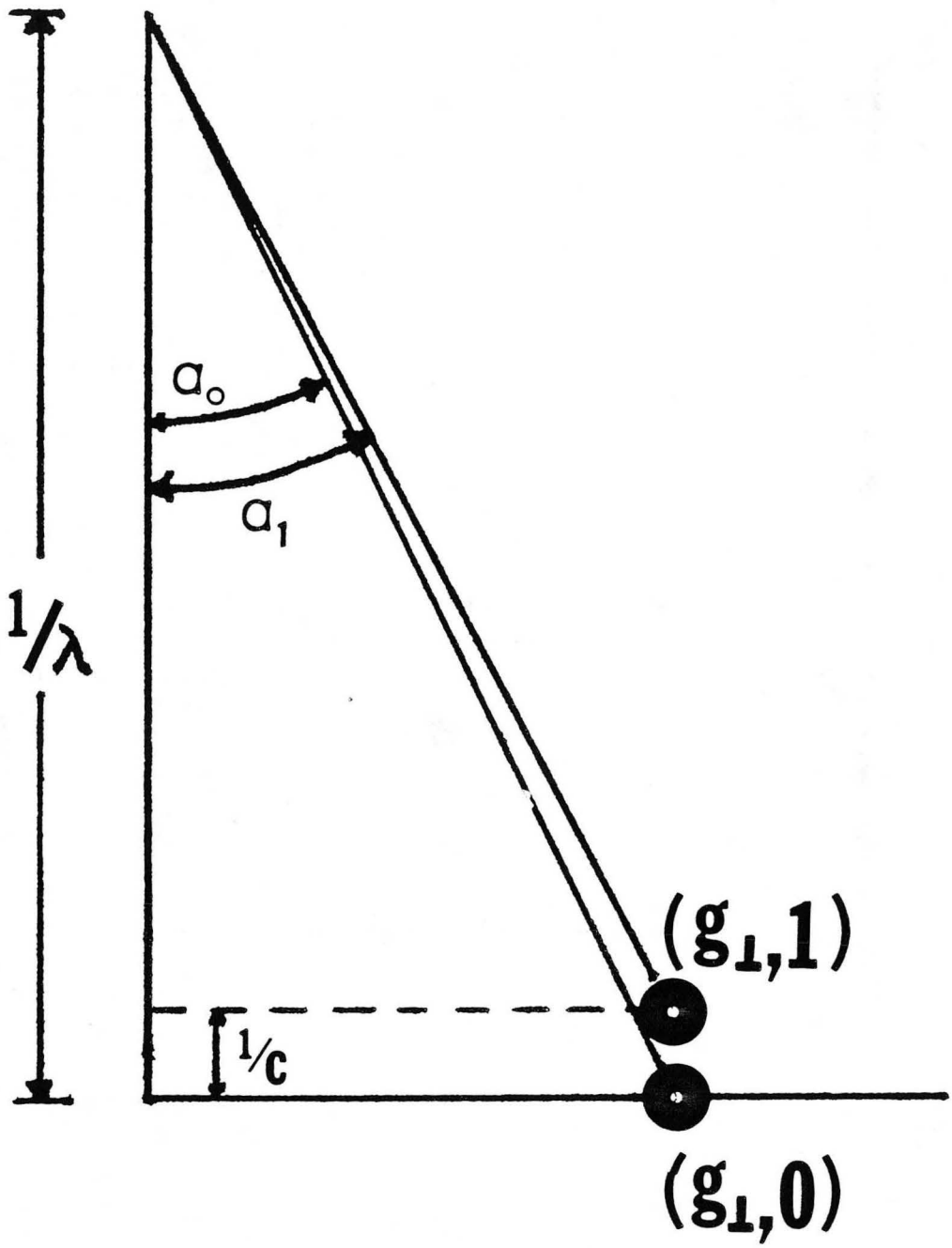


XBL 851-981

Figure 7

## Appendix A

The phase that appears in the exponent of the propagator is the difference in phase associated with electrons traveling a distance $\Delta z$ having a wavevector $\mathbf{k}_0$ relative to those having a wavevector $\mathbf{k}_1$ as shown in Fig. 6. This phase difference is equal to

$$\Delta\phi = |\mathbf{k}_1| \frac{\Delta z}{\cos\alpha} - |\mathbf{k}_0| \Delta z = k_0 \Delta z\left(\frac{1}{\cos\alpha} - 1\right) \approx \tfrac{1}{2} k_0 \Delta z \alpha^2 \tag{A1}$$

For electrons reflected into the first order Laue zone the angle $\alpha_0$ is equal to, see Fig. 7.

$$\alpha_0 = \frac{g_\perp}{1/\lambda} = g_\perp \lambda \tag{A2}$$

while for electrons scattered into the first order zone, the angle is

$$\alpha_1 = \frac{g_\perp}{1/\lambda - 1/c} \approx g_\perp \lambda\left(1 + \frac{\lambda}{c}\right) \tag{A3}$$

This gives a phase change of

$$\Delta\phi_0 = \tfrac{1}{2} k_0 \Delta z (g_\perp \lambda)^2 = \pi\lambda\Delta z g_\perp^2 = 2\pi\Delta z \xi(g_\perp) \tag{A4}$$

for electrons scattered into $(g_\perp,0)$, and a phase change of

$$\Delta\phi_1 = \tfrac{1}{2} k_0 \Delta z (g_\perp \lambda)^2 \left(1 + \frac{\lambda}{c}\right)^2 = \pi\lambda\Delta z g_\perp^2 \left(1 + \frac{\lambda}{c}\right)^2 \tag{A5}$$

for electrons scattered into $(g_\perp,1)$. The quantity $\xi\,(g_\perp) = 1/2\lambda g_\perp^2$ is the excitation error of the reflection $(g_\perp,0)$ and corresponds to the distance between the reciprocal lattice point $(g_\perp,0)$ and the Ewald sphere measured along the line connecting the center of the sphere with the reciprocal lattice point, see Fig. 1. The error in the phase of the propagator by using the excitation error of the zero order reflection instead of the the excitation of the first order reflection is thus

$$\Delta\phi_1 - \Delta\phi_0 = 2\pi\lambda^2 \Delta z g_\perp^2 / c \tag{A6}$$

As can be seen from (A6) the error depends on slice thickness and electron wavelength and goes to zero as $\Delta z$ and $\lambda$ goes to zero.

This report was done with support from the Department of Energy. Any conclusions or opinions expressed in this report represent solely those of the author(s) and not necessarily those of The Regents of the University of California, the Lawrence Berkeley Laboratory or the Department of Energy.

Reference to a company or product name does not imply approval or recommendation of the product by the University of California or the U.S. Department of Energy to the exclusion of others that may be suitable.

*LAWRENCE BERKELEY LABORATORY*
*TECHNICAL INFORMATION DEPARTMENT*
*UNIVERSITY OF CALIFORNIA*
*BERKELEY, CALIFORNIA 94720*